AIAA-2025-1489

Interactions of Controlled Streamwise Vortices with a Turbulent Boundary Layer

Barnabas Toth[1], Bojan Vukasinovic[2] and Ari Glezer[3]
Georgia Institute of Technology, Atlanta, GA 30332-0405

Matthew C. DeFore[4] and Chris Harris[5]
Northrop Grumman Aeronautics Systems

The interactions of circular and rectangular surface jets having the same orifice area with a flat plate turbulent boundary layer [TBL, $Re_x = O(10^6)$] in a uniform stream are compared in wind tunnel investigations where the characteristic length scales of the jets' orifices are an order of magnitude smaller than the boundary layer thickness. Each surface jet is formed over a range of momentum coefficients and issues at a pitch angle $\alpha = 20°$ and several yaw angles $45° < \beta < 90°$ (in addition to $\beta = 0°$). It is shown that as a result of the different orifice geometries the interactions of the jets with the cross-flow boundary layer are significantly different and result in notably distinct flow structures. Specifically, while the circular jet leads to the formation of a pair of asymmetric counter-rotating streamwise vortices above the surface whose symmetry varies with the yaw angle, the rectangular jet leads to the formation of a single surface-bound streamwise vortex owing to the Coanda effect along its long side. It is shown that the formation of the surface bound single-sign vortex by the rectangular jet remains close to the surface and its spanwise effects on enhanced streamwise momentum flux, entrainment and mixing in the surrounding boundary layer flow are significantly more pronounced than those for the corresponding streamwise vortices that are formed by the circular jet, which exhibits a higher rate of streamwise decay.

Nomenclature

A_j	=	orifice cross-sectional area	ρ	=	air density
α	=	jet pitch	θ	=	BL momentum thickness
β	=	jet yaw	U	=	local velocity component
C_μ^F	=	momentum/force coefficient	U_0	=	freestream velocity
d	=	(equivalent) jet diameter	ω_x	=	streamwise vorticity component
δ	=	boundary layer thickness	x	=	direction along the surface
$\vec{F}$	=	jet trust	y	=	direction normal to the surface
Γ	=	circulation	z	=	direction across the span
q	=	turbulent kinetic energy	$\widehat{\varphi}$	=	streamwise momentum flux
Q	=	volumetric flowrate			

1 Graduate Research Assistant, AIAA Member.
2 Research Engineer, AIAA Member.
3 Professor, AIAA Fellow.
4 Sr. Engineer, AIAA & INPSI Member.
5 Technology Development.

I. Introduction

Jets in cross flow are ubiquitous in a broad range of applications and have been studied extensively in numerous configurations over the years (e.g., Margason, 1993). The classical and most thoroughly studied example of jets in crossflow is the transverse jet, issuing normal and aligned in the direction of the cross flow where the boundary layer interaction with the jet results in the formation of a pair of counter-rotating vortices along the spanwise edges of the jet. Early investigations of the flow were motivated by atmospheric mixing, but they have rapidly evolved to include flows related to species mixing, cooling, aerodynamic maneuvering, etc., as outlined in detailed review articles by Mahesh (2013), Karagozian (2014), and Sharmishtha and Utpal (2017).

Motivated by interest to utilize jets in cross flows as 'active' vortex generators in boundary layers over solid surfaces, Johnston and Nishi (1990) used surface-inclined jets for the deliberate formation of streamwise vortices of prescribed sense. They produced configurations of co- and counter-rotating vortices by using inclined surface actuation jets that are yawed relative to the direction of the cross flow and noted the effect of jet yaw on delaying separation. In a later investigation, Compton and Johnston (1992) studied the effects of yaw angle and velocity ratio of an inclined jet on the vorticity and circulation of the ensuing dominant streamwise vortex and reported that stronger vortices were formed at yaw angles between 45^o and 90^o, and at higher velocity ratios. In a later review of vortex generator jets, Johnston (1999) noted that strong, single-sense vortices are formed by inclined jets at pitch angles below 45^o that are yawed within 60^o and 90^o. Bray and Gary (1999) developed parametric fit expressions that relate vortex circulation to the jet pitch and yaw, mass flow rate, and its plenum pressure. In a later study Milanovic and Zaman (2003) measured the flow downstream of highly inclined jets in a flat plate boundary layer over a range of yaw and pitch angles, jet momentum ratio and boundary layer thickness and characterized the peak streamwise vorticity noting that highly yawed jets remain closer to the surface, enhance the turbulence intensity within the boundary layer, and reach their peak vorticity farther downstream. Rixon and Johari (2003) showed that the circulation of streamwise vortices that are contained within the boundary layer increases linearly with jet velocity ratio when the vortices are overlaid. More recently, Feng et al. (2018) proposed a model that predicts the evolution of a jet in a cross flow based on its pitch and yaw angles and velocity ratio, and argued that the evolution of the ensuing single-sense vortex in the far-field is an extension of the jet in that its penetration and circulation increase and decrease as 1/3 and -1/3 power of the streamwise distance, respectively.

In contrast to the circular jet, the jets in crossflow out of rectangular orifices have been studied less. Most of the early work, reviewed by Gutmark and Grinstein (1999), was motivated by mixing enhancement and the jet dynamics in the orifice vicinity. Motivated specifically by boundary layer flow applications and streamwise vortex generation, Zhang (2000) considered pitch of 30° and yaw varying from 0° to 135° that resulted in vortices exceeding the boundary layer height while their cores were contained within. He has shown that, in comparison, rectangular jet can produce a stronger vortex than one with a circular orifice for a yaw of 90°. At the same time, the yaw of the rectangular jet yielding the highest circulation was considered to be around 75°, although somewhat dependent on downstream position. Interestingly, Godard et al. (2006) arrived at the same conclusion for rectangular jets issuing at a 90° pitch configuration in an adverse pressure gradient, where they observed that skin friction increased with decreasing yaw. Recently, Tricouros et al. (2023) performed a parametric study of various factors for rectangular pitched and yawed jet issuing into a laminar boundary layer. They concluded that for the purposes of energizing the boundary layer,

a higher aspect ratio and to a lesser degree, a higher yaw angle was beneficial.

While many aspects of the evolution of inclined yawed jets in cross flow have been investigated since the 1990s, few prior investigations considered the evolution of jets within a turbulent boundary layer having a characteristic scale that is significantly larger than the scale of the jet. The present investigations build on an earlier study by Toth et al. (2024) that specifically focused on the interactions of pitched and yawed jets with a nominally 2-D cross flow over a flat plate such that the resulting jet-induced vortical structures remain bounded within the turbulent boundary layer. This was done with specific attention to streamwise changes in momentum flux and turbulent characteristics, as well as the structure and strength of the streamwise vorticity concentrations relative to the base flow. The present work examines differences and similarities between jets issuing through circular and rectangular orifices with respect to the vortical flow composition and its spatial evolution, along with their ramifications on the redistribution of the boundary layer momentum flux.

II Experimental Setup and Flow Diagnostics

The present investigations are conducted in an open-return, low-speed wind tunnel (Figure 1) driven by a 150 HP blower (up to 95,000 CFM) with a 10:1 contraction downstream of a turbulence management section having a square test section measuring 106 cm on the side and 304 cm in length. The bottom wall of the test section was replaced with a horizontal flat plate model that can be translated vertically. The tunnel's test section is optically transparent from three sides to enable optical measurements using PIV and flow visualization. Prior to the installation of the flat plate model, the flow uniformity across the tunnel's test section was verified using Pitot probe measurements over a square grid at a range of crosswind speeds. The flat plate model is fabricated from a monolithic composite having a honeycomb core, sandwiched between two aluminum plates. The plate spans the full width of the tunnel's test section and is designed to be mounted so that it splits the airflow downstream of the contraction (Figure 1) to form a spanwise-uniform boundary layer over its upper surface downstream of a bullnose half cylinder leading edge. The plate is attached on its lower surface to a light aluminum frame connected to four electric risers to enable adjustment of its elevation and streamwise inclination within the test section. Although in the present experiments the plate orientation is horizontal (zero pressure gradient), it is also possible to accommodate small favorable and adverse streamwise pressure gradients. The plate incorporates an interchangeable cylindrical jet module that forms an inclined yawed jet of diameter d relative to the cross flow (about 1,150d downstream from the plate's leading edge). In the present investigation, main stereo

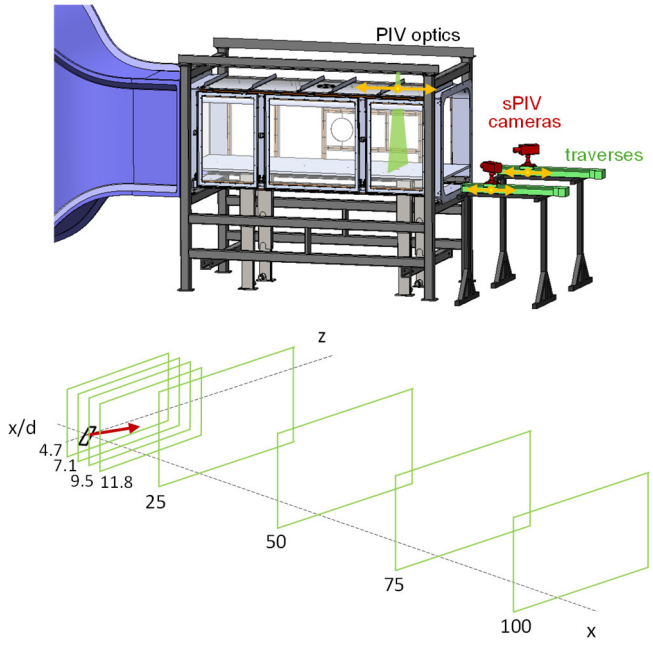

Figure 1. *Schematics of the experimental setup, and the sPIV measurement planes.*

PIV (sPIV) measurements are acquired in the three streamwise-normal *y*-*z* planes $x/d = 25$, 50, 75 and 100 (relative to the downstream edge of the jet orifice) and the nominal PIV optical setup is shown in Figure 1. In addition, a limited sPIV is also conducted immediately downstream from the jet orifice, at $x/d = 4.7$, 7.1,9.5 and 11.8. In all measurement planes, the spatial vector-resolution of the flow field is kept at about $0.8d$.

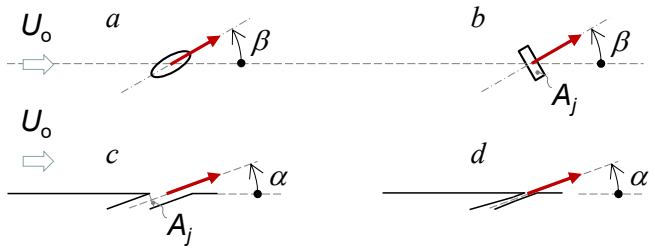

Figure 2. *Top (a,b) and cross-sectional (c,d) views of the circular (a,c) and rectangular (b,d) jet orifice (A_j) geometries, having the pitch (α) and yaw (β) directions marked.*

As one of the main objectives for this work is comparison between the circular and rectangular jets, two jet geometries are selected (Figure 2). Based on the prior investigation on round jets (Toth et al., 2024), the jet pitch is set to $\alpha = 20°$ for both jets, while the orifice cross-sectional area A_j is kept the same, resulting in the same jet characteristic dimension $d = d_{eq}$, hence a simpler notation d is retained for the rest of the paper. The jet geometry is formed within interchangeable cylindrical modules that are fabricated using stereolithography and are flush-mounted into the mating opening in the plate. The design enables continuous variation of the jet's yaw angle β relative to the free stream. Based on the earlier study on round jets (Toth et al., 2024), the yaw angles of interest span a quadrant bound by $\beta = 45°$, 60°, 75°, and 90°, in addition to the reference $\beta = 0°$. In the present investigations, the jet characteristic parameter is defined as the ratio of the jet momentum flux (based on the force, hence C_μ^F, not C_μ) to the boundary layer momentum flux (rather than by the conventional ratio of the jet momentum to the outer flow momentum). The force-based jet momentum flux (or jet force) $\vec{F}$ is measured directly in bench tests outside of the tunnel in the absence of cross flow using a 3-axis load cell over a range of independently measured jet mass flow rates. The total force F effected by the jet is resolved on two axis of load cell and is subsequently used to define a momentum coefficient $C_\mu^F = F/\left(\rho \cdot U_0^2(\delta - \theta) \cdot d_{eq}\right)$, where the denominator represents the momentum flux within the boundary layer across the jet orifice characteristic scale. The coefficient C_μ^F thus serves as a measure of the aerodynamic load the jet imposes only on the boundary layer over the jet orifice and hence this coefficient is typically of the order O[1]. Figure 3a illustrates the measured boundary layer profiles at all four main measurements planes (x/d = 25, 50, 75, and 100), while Figure 3b shows the jet calibration results for both the circular and rectangular jets. In addition, the corresponding calibration results for the circular jet used by Toth et al. (2024) are included for reference. Lastly, all the present studies are conducted at a fixed jet flow rate, which resulted in slightly different jet

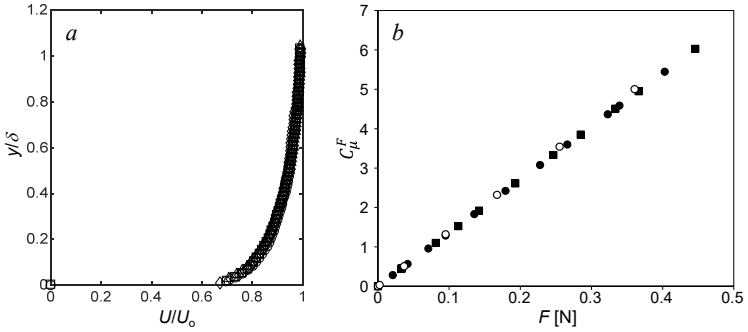

Figure 3. *Boundary layer mean velocity profiles (a) at x/d = 25 (Δ), 50 (□), 75 (○), and 100 (◊), and jet momentum coefficient relative to the total jet force in the absence of crossflow for the circular (●) and rectangular (■) jet orifice. Corresponding jet momentum coefficients for the circular (○) jet (Toth et al., 2024) are shown for reference.*

momentum/force coefficients of $C_\mu^F = 3.2$ for rectangular and $C_\mu^F = 3.1$ for the circular jet.

III. Interactions of Pitched/Yawed Jets with the Boundary Layer

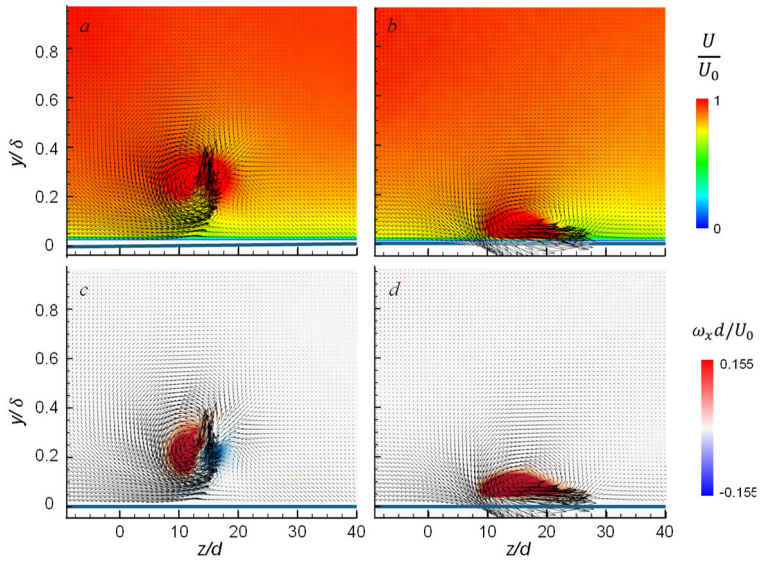

Figure 4. *Color raster plots of the mean streamwise velocity (a,b) and vorticity (c,d) for the circular $(a, c,\ C_\mu^F = 3.1)$ and rectangular $(b, d,\ C_\mu^F = 3.2)$ jet interaction with the boundary layer at x/d = 25, and the jets' yaw angle $\beta = 60°$.*

To initially emphasize the differences between circular and rectangular jet interactions with turbulent boundary layer flow, two characteristic instances are shown in Figure 4, where the mean in-plane velocity field is complemented by a color raster plot of the mean streamwise velocity component in Figures 4a and b, as measured at $x/d = 25$. As a representative case, the yaw angle relative to the boundary layer flow is $\beta = 60$, while the jets' force momentum coefficient is $C_\mu^F \approx 3.2$. Several notable differences are seen in the flow fields. As already pointed out by Toth et al. (2024), a circular jet's main interaction domain shifts towards the surface with decreasing jet pitch angle. Nonetheless, as also seen in Figure 4a, it is still somewhat displaced off the surface ($y = 0$) even at this low pitch angle $\alpha = 20°$, while the peak streamwise velocity domain appears bimodal. In contrast to the circular jet, interaction of the rectangular jet (Figure 4b) remains confined to the surface, having a single domain of the streamwise velocity gain from the jet. In addition, it is also clear that the interaction domain of the rectangular jet is deflected sideways, since it is centered at about z/d = 17, compared to the circular-jet domain at about z/d = 14. Another important difference is reflected in the dominant in-plane velocity direction, which, in the case of the circular jet points away from the surface and nearly upward, while the prevailing velocity of the rectangular jet interaction is sideways, indicating a stronger transport of the low momentum fluid near surface towards the bulk BL flow in the former. Complementing the topological flow features in Figures 4a and b, the corresponding mean streamwise vorticity concentrations reveal the differences in vortical flow compositions of these two jet interactions in Figures 4c and d. Again, as previously discussed in greater detail by Toth et al. (2024), although it is widely considered that inclined and yawed circular jet induces a single-sense (CCW) streamwise vortex in its interaction with BL flow, it is seen that its pair (CW) vortex remains in the extended downstream interaction domain (Figure 4c), while the CW vortex weakens along the way and ultimately loses its coherence. Contrary to this scenario, rectangular jet (Figure 4d) does induce a single-sense (CCW) vortex even at x/d = 25, and the streamwise velocity/momentum gain (Figure 4b) is clearly associated with the dominant vortex domain seen in Figure 4d.

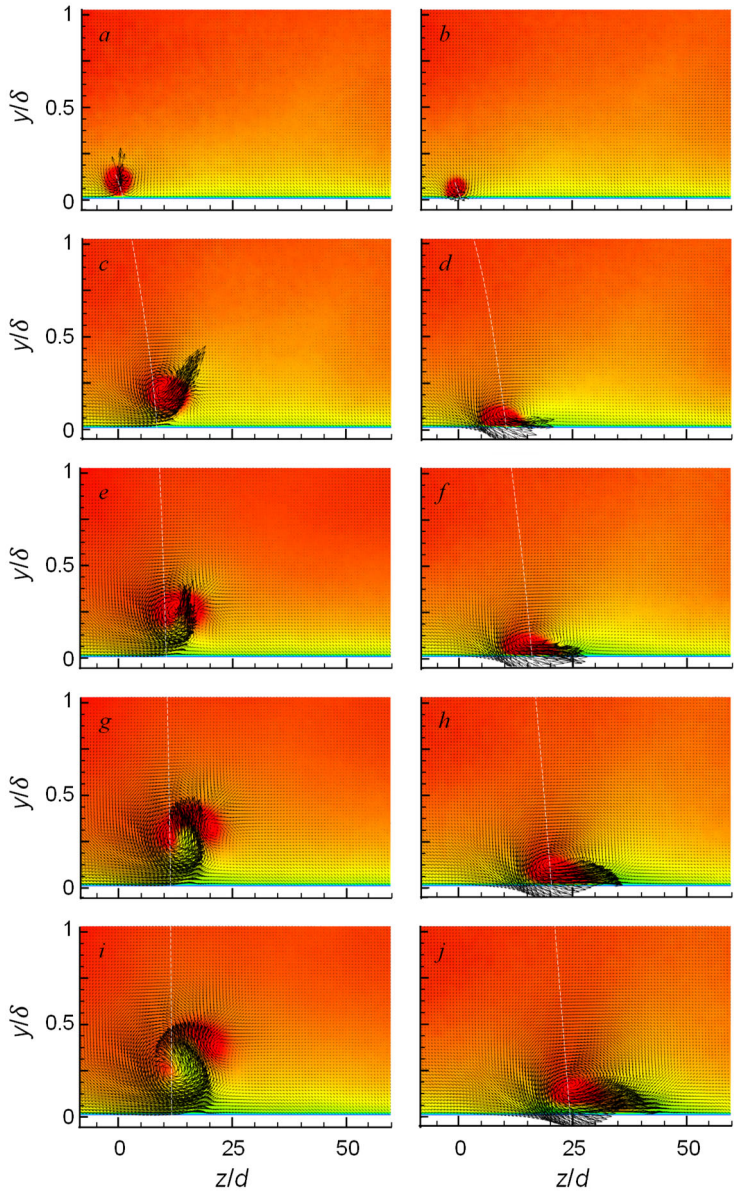

Figure 5. *Color raster plots of the mean streamwise velocity for the circular (a, c, e, g, i, $C_\mu^F = 3.1$) and rectangular (b, d, f, h, j, $C_\mu^F = 3.2$) jet interaction with the boundary layer at x/d = 25, and the jets' yaw angle β = 0° (a,b), 45° (c,d), 60° (e,f), 75° (g,h), and 90° (i,j). Colorbar range is the same as in Fig. 4.*

Assessment of the yaw angle influence on this initial jet-BL interaction is shown in Figure 5 in terms of the spatial distributions of all three mean velocity components. Following the findings of Toth et al. (2024) on a tradeoff between the momentum gain and vortex circulation with the yaw orientation, the present study focuses on the range of the yaw angles $45° \leq \beta \leq 90°$. In addition, the zero-yaw case is also shown for reference. Both zero-yaw flow fields (Figures 5a and b) indicate direct jet contributions in the streamwise velocity/momentum, centered about the jet orifice (z/d = 0). At $\beta = 45°$, the main momentum contribution for the circular jet (Figure 5c) shifts sideways to about z/d = 10, while being concentrated in a single domain, accompanied by a strong in-plane component of velocity away from the surface. While the signature of the jet is also concentrated in a single domain for the rectangular jet (Figure 5d), and similarly displaced sideways, the notable difference is in that this domain is near the surface. As already seen in Figure 4a, interaction domain for the circular jet at $\beta = 60°$ (Figure 5e) exhibits a dual lobe, where the side with CCW sense of rotation dominates the CW side. Along with further increase in the yaw angle to $\beta = 75°$ (Figure 5g) and $\beta = 90°$ (Figure 5i), this asymmetry amplifies, with other notable evolution that the momentum gain shifts to the side of the weaker CW motion of the pair. Compared to the noted changes in the circular jet interactions with the BL flow, there is a much weaker effect of the yaw angle on the interactions of the rectangular jet (Figures 5 d, f, h, and j). While there is a single CCW sense of rotation for any yaw angle, the angle effect is seen predominantly in the structure growth with β. Vortices remain mostly along the surface up to the highest yaw angle (Figure 5j), where a minimal vortex displacement becomes visible. As it can be expected due to the vortex kinematic mirroring to form a stagnation "surface" (in between the two mirrored vortices), the shorter vortex distance

from the wall implies a higher self-induced velocity, which in the case shown in Figure 5 suggests a stronger vortical sideways deflection for the rectangular jet. Clearly, a higher sideways vortex displacement is seen in all the nonzero yaw cases for the rectangular jet, which is emphasized by white dashed lines.

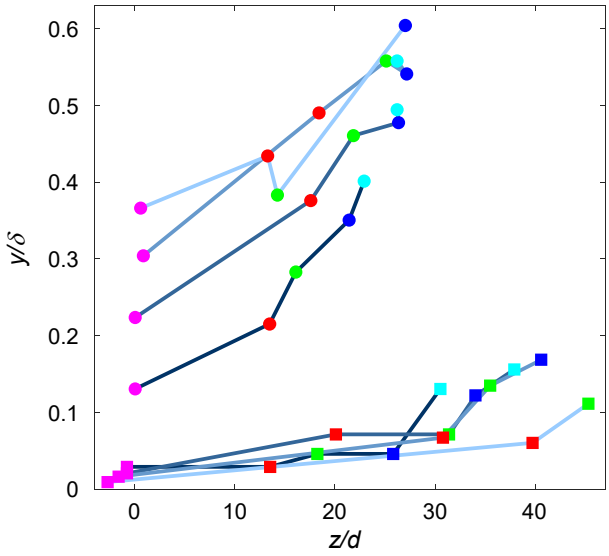

Figure 6. *Trajectories of the peak jet momentum for the circular (●) and rectangular (■) jet orifice at streamwise positions x/d = 25 (—), (b) 50 (—), 75 (—) and 100 (—), for jet yaw β = 0° (●, ■), 45° (●, ■), 60° (●, ■), 75° (●, ■), and 90° (●, ■).*

Assuming that the main signature of the jet contribution is expressed through the peak streamwise velocity increase, the jet trajectories are followed through all four streamwise measurement planes (x/d = 25, 50, 75, and 100), and for all the jets' yaw angles. Figure 6 summarizes the captured differences in the jets' deflections across the span and away from the surface. A clear separation between the trajectories of circular vs. rectangular jets for all the cases further amplifies significantly different jet interactions with the BL flow. The circular jet at zero yaw progressively lifts off the surface in the streamwise direction with practically no sideways drift. For all the other nonzero yaw angles, circular jets progress in the streamwise direction with both the upward and sideways deflection. However, the sideways deflection diminishes with the yaw angle, particularly at the two highest yaw angles, indicating that the jet issuing at higher yaw angle converts that momentum into the streamwise closer to the jet origin. As previously seen in the loss of velocity/momentum at these angles at x/d = 25 (Figure 5), it can be argued that this quick turn comes at the expense of increased losses. Contrary to circular jets, rectangular jet interaction is mainly expressed in the sideways jet deflection with the yaw angle, in some instances even doubling the sideways deflection of the circular jets. Moreover, the difference in the upward deflection is even greater. Regardless of the yaw angle, most of the jets remain within 10% of the BL thickness even down to a hundred diameters downstream from the jet issuance. A significantly stronger dependence of the jet upward deflection on the yaw angle is seen for the circular jets, in spite of dampened nature of the deflection magnitude with the increase in the yaw angle. Even though these deflections extend past half the BL thickness, compared to only 10% for the rectangular jet, it needs to be emphasized that they remain well within the BL bounds.

Further analysis characterizes the spanwise effect of a single jet on the turbulent boundary layer flow. First, an integral measure of the increment of the cross-stream magnitude of streamwise momentum flux at spanwise positions z is defined as $\Delta\varphi(z)$, relative to the base flow in the absence of the jet. Figure 7 shows spanwise distributions of the normalized $\Delta\widehat{\varphi}(z) = \delta\cdot\Delta\varphi(z)/F$ (where δ is the boundary layer thickness of the base flow and F is the magnitude of the jet force, c. f., Figure 3b) for both jets and the yaw angles β = 0°, 45°, 60°, 75°, and 90°. While such distributions are shown for all the measured planes for rectangular jet, analogous results for the circular jet are shown only for the two farthest measurement planes for comparison with rectangular jet, as similar

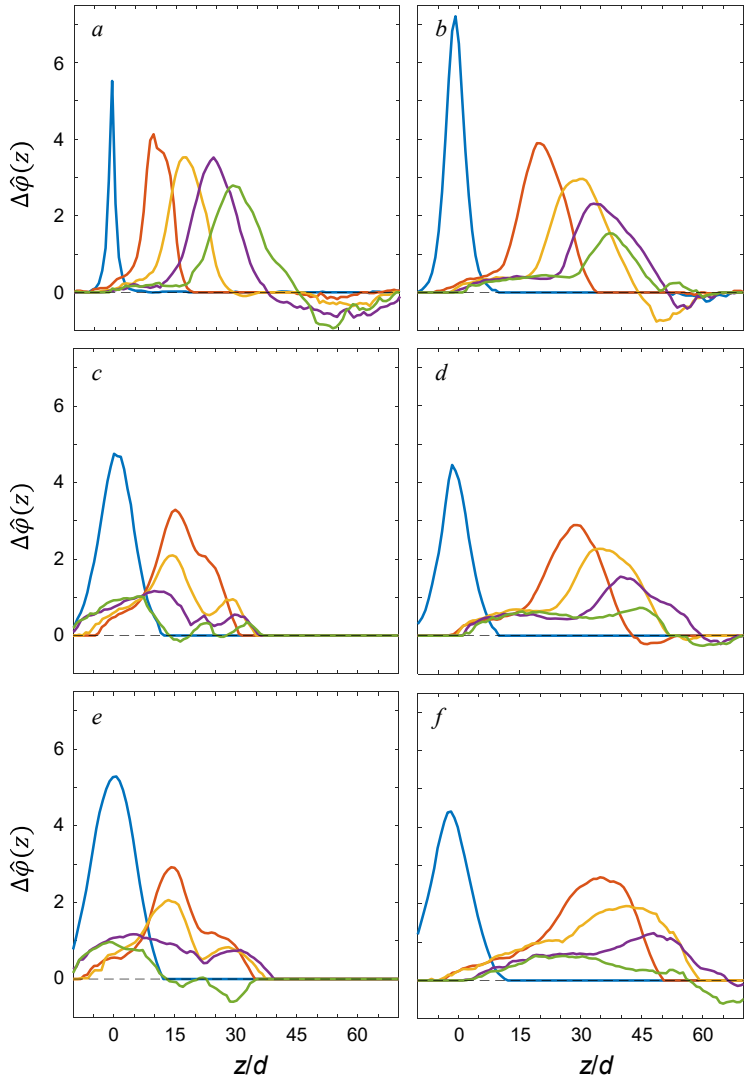

Figure 7. *Distribution of spanwise momentum increments ΔΦ at streamwise positions x/d = 25 (a), 50 (b), 75 (d), and 100 (f) for the rectangular jet (C_μ^F=3.2,), as well as x/d = 75 (c) and 100 (e) for the circular jet (C_μ^F=3.1), for the range of yaw angles β = 0° (—), 45° (—), 60° (—), 75° (—), and 90° (—).*

discussion of these distributions was already presented by Toth et al. (2024) for circular jets. The distributions of $\Delta\hat{\varphi}(z)$ for rectangular orifice yaw $\beta = 0$ at the first two downstream planes (Figures 7a and b) show narrow symmetric distributions about $z/d = 0$. While all the distributions shift sideways with increasing yaw angle owing to the jet interaction shift seen in the flow fields, they remain fairly symmetric in all the cases measured in the closest plane (Figure 7a). It is also noted that due to the increased interactions with cross flow and incurring losses, the peak momentum gain diminishes with yaw, while promoting spreading across the span. It is also noted that extents of small but traceable momentum deficit relative to the base BL flow are seen at the end tails of these distributions (typically past z/d = 45). By the next measurement plane (Figure 7b), continuing shift across the span is seen, with a very little difference in the distribution shapes, but with a further reduction in the peak gains and an increase in spreading. As already stated, comparison between the circular and rectangular jets focuses on the two most downstream planes (x/d = 75 and 100) in Figures 7c and d, and Figures 7e and f, respectively. In general, both circular and rectangular jets indicate similar dependence on the yaw angle. While zero yaw cases indicate persistent direct contribution by the jets, the yawing effect indicates redistribution of the direct jet momentum across the span, having lower peak momentum flux with expanding spanwise distribution. In principle, yaw angles $\beta = 45°$ and 60° indicate more favorable net gain effect across the span relative to $\beta = 75°$, and in particular when compared to the case of $\beta = 90°$. Besides the already noted wider spanwise spreading of the momentum flux gain for the rectangular jet, the distributions at $x/d = 100$ (Figures 7e and f) suggest that the jet effect may begin to diffuse sooner for the circular jet, as the net gain at $\beta = 45°$ and 60° remains strong for rectangular jet, while the effect of the circular jet somewhat weakens.

While the momentum flux analysis presented in Figure 7 quantifies a global net gain in the

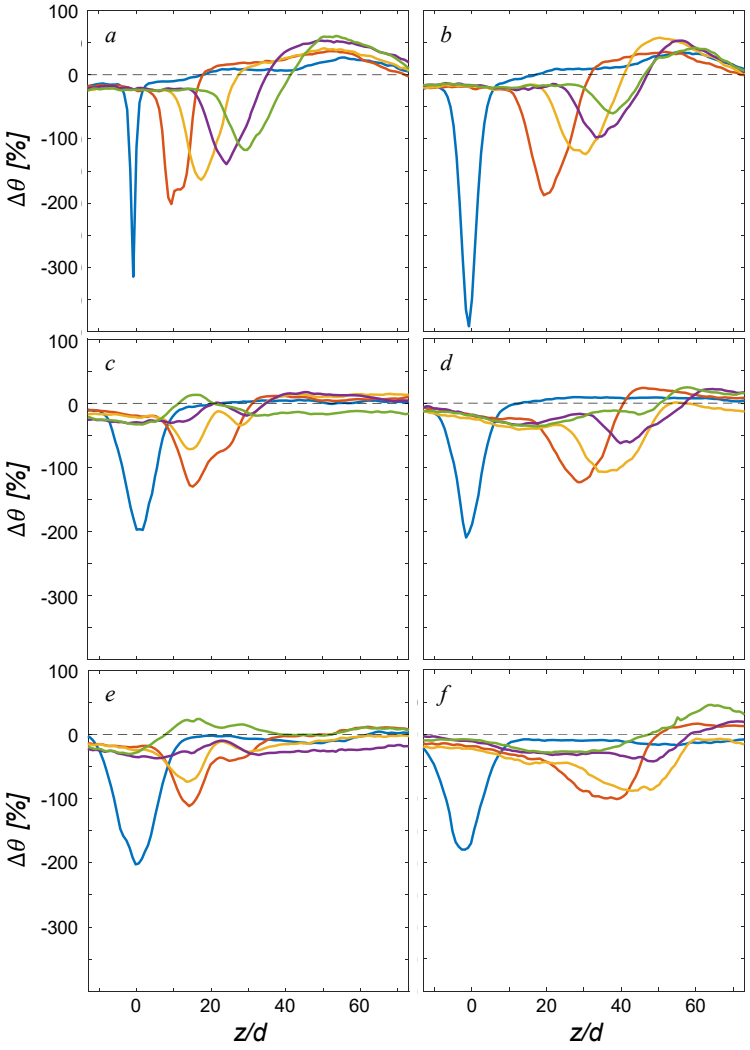

Figure 8. *Distribution of relative momentum thickness increment Δθ [%] at streamwise positions x/d = 25 (a), 50 (b), 75 (d), and 100 (f) for the rectangular jet (C_μ^F=3.2,), as well as x/d = 75 (c) and 100 (e) for the circular jet (C_μ^F=3.1), for the range of yaw angles β = 0° (—), 45° (—), 60° (—), 75° (—), and 90° (—).*

streamwise momentum flux, another parameter is sought for quantification of the jet effectiveness from the standpoint of the BL momentum – momentum thickness θ. Similar to the analysis presented in Figure 7, Figure 8 shows spanwise net change in the momentum thickness of the boundary layer with and without interaction with circular and rectangular jets, for the same five jet yaw angles. To preserve the one-to-one comparison with the results shown in Figure 7, Figure 8 also shows such distributions across all four streamwise measurement planes (x/d = 25, 50, 75, and 100) for the rectangular jet, while the comparison with the circular jet is done in the farthest two measurement planes. As expected, a very sharp and narrow reduction in the BL thickness is attained symmetrically about z/d = 0 for the rectangular jet in the first measurement plane (Figure 8a). As the yaw angle increases, the effect on the BL thickness shifts sideways, with the decreasing minimum and widening extent. At the same time, the zero crossing and net increase in the θ shift sideways as well. The two competing effects are clearly seen on two sides of the streamwise vortex, as the magnitude of the increase in θ also becomes amplified with the increase in yaw. By the next measurement plane (x/d = 50), shown in Figure 8b, each distribution of the net change in momentum thickness continues to spread and decreases in peak. On the side of the momentum thickness increase, no appreciable change in magnitude is noted in this plane. However, at the next measurement plane for rectangular jet (Figure 8d), net gain effect appears to subside, along with the overall stronger dependence on yaw angle, as the net benefit from the jet oriented at β = 90° significantly weakens, while the others continue the spreading and diminishing in the peak magnitude. When compared to the corresponding effect of the circular jet (Figure 8c), it is seen that the jet effect weakens much more for the circular jet, as the effects of the jet at both β = 75° and 90° become significantly diminished, while even the jet oriented at β = 60° induces distinctively smaller effect than its counterpart rectangular jet. Finally, these differences only

become amplified at the last measurement plane (x/d = 100). By this plane, the rectangular jet oriented at $\beta = 45°$ and 60° (Figure 8f), significantly outperforms the circular jet (Figure 8e) with respect to the momentum thickness decrease, having an average decrease of 39% across the measured span for the rectangular jet, compared to a 19.5% average reduction of θ by the circular jet for the $\beta = 60°$ case Hence, this analysis of the evolution of θ suggests more strongly than the momentum flux analysis that the net positive effect of the rectangular jet persists further downstream from the jet issuance than in the case of the circular jet, particularly for the yaw angles $\beta = 45°$ and 60°.

IV The Jet-Induced Vortical Structures

As discussed in §III, the interaction of pitch and yawed jet with a cross flow results in the formation of streamwise vortices along the spanwise edges of the jet and their signatures depend on the yaw (and pitch) angle, as also previously assessed by Toth et al. (2024). To isolate the evolution of these vorticity concentrations within the flow is assessed using the Γ_1 criterion (Graftieaux et al. 2001, Berson et al. 2009) to define the centers and bounds of vorticity concentrations. When applied to the flow fields in Figure 5c-j, the embedded vortical structures are isolated, as shown in Figure 9, where only the extracted vortex contours are shown, along with raster plots of vorticity magnitude within these bounds. As already mentioned, the streamwise velocity/momentum gain due to the rectangular vortex interaction remains concentrated near the surface for all the tested yaw angles (c.f., Figure 6), Figures 9a–d clearly show that a single-sense CCW vortex, resulting from the rectangular jet interaction with the BL flow, is associated with these domains. In addition, the vortex spatial extent grows with the yaw angle, which certainly affects its circulation, as it is quantified later. It is also known, both from the present work and prior work by Toth et al. (2024), circular jet interaction with the BL flow results in dual vortical composition, where a dominant CCW vortex is accompanied by its CW vortex pair, as also seen in Figures 9 e–h. At the lowest yaw angle $\beta = 45°$ (Figure 9e), the vortex pair tilt is close to 45 degrees relative to the surface, inducing the upwash of the near surface fluid in that common direction for the vortex pair. In

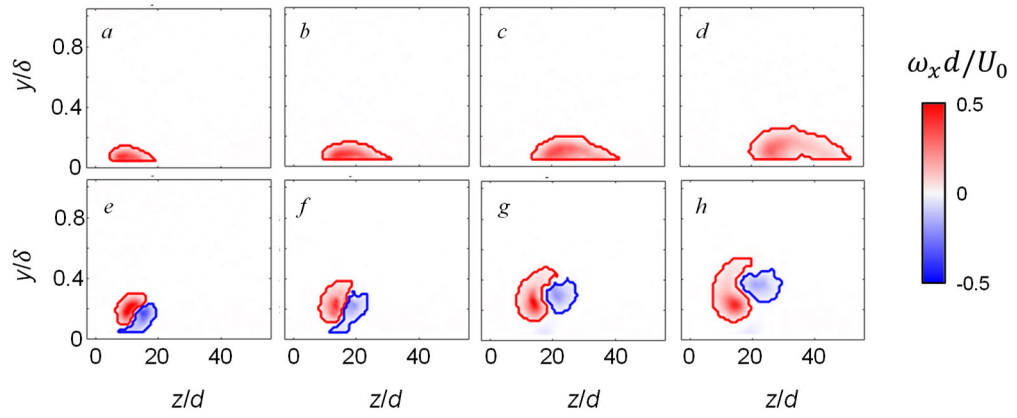

Figure 9. *Color raster plots of the time-averaged streamwise vorticity at x/d = 25 downstream from the rectangular (a–d, C_μ^F=3.2) and circular (e–h, C_μ^F=3.1) jets for the yaw angles β = 45° (a,e), 60° (b,f) , 75° (c,g), and 90° (d,h), having the detected CCW (red) and CW (blue) vortical domains marked.*

addition, the induced velocities by each vortex onto the other tend to propel them in the same direction, away from the surface, while being swept in the downstream direction by the BL flow. Due to imbalance in circulation, it can be also expected that the weaker CW vortex becomes

wrapped around its CCW pair. With the increase in yaw angle (Figures 9 f–h), several trends in the vortical evolution are noted. First, both vortices become progressively more displaced away from the surface, arguably due to the increase in circulation and stronger self-induced velocities. Also, the disparity in circulations between CCW and CW vortex likely increases, as the CW vortex becomes increasingly wrapped around the dominant CCW vortex, which also results in their joint induced velocity being close to normal to the surface, transporting the near-surface fluid even more directly upward, when compared to the $\beta = 45°$ orientation. Moreover, at the highest yaw angle (Figure 9h), the vortex pair tilt appears to change the slope. Overall, the most striking differences between the circular and rectangular jet interactions are the dual vs. singular resulting vortical composition of the flow, with associated close adherence to the surface of the rectangular jet-induced CCW vortex regardless of the jet's yaw orientation.

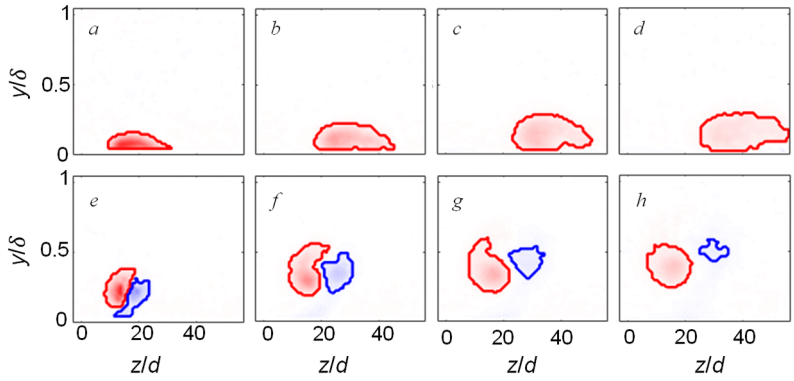

Figure 10. *Color raster plots of the time-averaged streamwise vorticity at x/d = 25 (a,e), 50 (b,f) , 75 (c,g), and 100 (d,h) downstream from the rectangular (a–d, C_μ^F=3.2) and circular (e–h, C_μ^F=3.1) jets for $\beta = 60°$. Contour levels are the same as in Fig. 9.*

To illustrate vortex evolution in the downstream direction, a representative yaw orientation $\beta = 60°$ is selected for both the rectangular and circular jet interactions. Analogous to Figure 9, only the vortex contours are extracted from the measured flow fields and the associated vorticity within the vortex bounds are plotted as color raster plots in Figure 10. As expected, all vortices diffuse along the downstream direction, but there are notable differences in the evolution of the dominant CCW vortex when formed by the rectangular and circular jets. There is consistent growth and diffusion of the CCW vortex all the way up to $x/d = 100$ (Figure 10d). Moreover, due to its proximity to surface, this vortex continues to deflect sideways, even becoming displaced at the very edge of the measurement domain at the most downstream location (Figure 10d), marking its sideways displacement about 1/3 of that in the downstream direction. It is also clear from Figures 10a–d that the strong sideways deflection is accompanied by a small but detectable motion away from the surface. Contrary to this scenario, the dominant CCW vortex created by the circular jet does not grow in the downstream direction as much as its rectangular-jet counterpart, reaching its maximum sideways displacement ($z/d \approx 16$) already at $x/d = 50$ (Figure 10f), and also reaching its asymptotic displacement away from the surface by $x/d = 100$ ($y/\delta \approx 0.4$, Figure 10h). Along the way, the weaker CW vortex gets moved around its CCW pair while their interaction weakens both of them. In turn, the weakened CCW vortex induces less displacement of the CCW vortex, eventually leading to the stated asymptotic displacement. Furthermore, although still present as a remnant at $x/d = 100$ (Figure 10h), the CW vortex nearly lost all of its coherence and the remaining CCW vortex (re)organizes towards a circular shape, as can be expected for a single streamwise vortex sufficiently isolated from surfaces and interactions with other vortices. It is emphasized at this point again that even at a hundred diameters downstream from the circular jet issuance, no exclusive single-sense vorticity is present, while the vortical evolution up to this point indicates the final stages of the interaction domain where both the CCW and CW vortices exist.

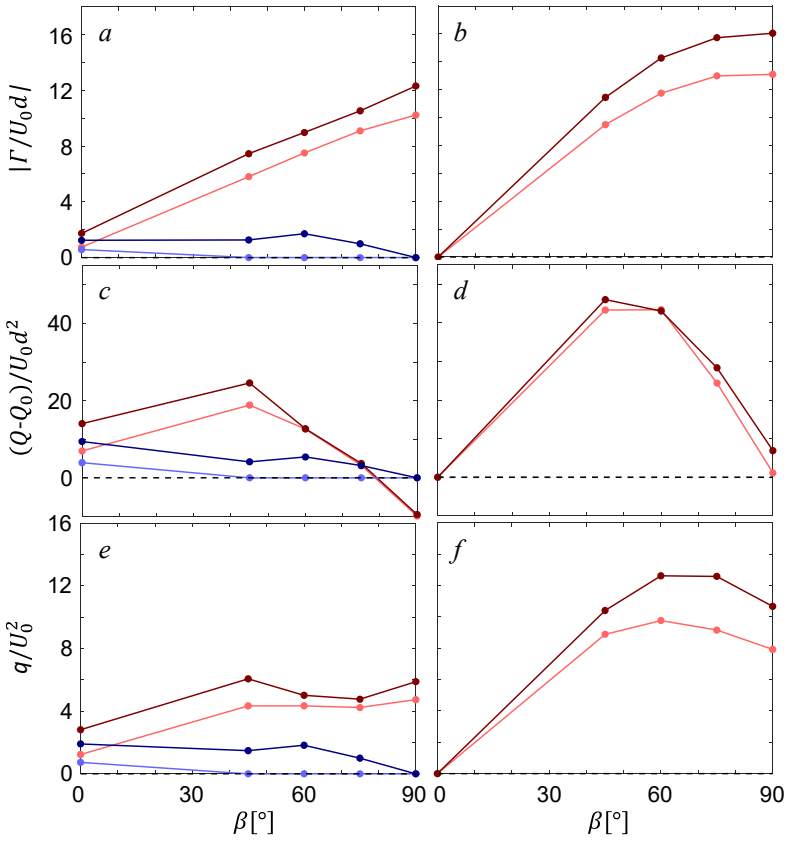

Figure 11. *Circulation (a-b), volumetric flow rate gain (c, d) and TKE (e, f) within the CCW (●) and CW (●) vorticity domains at x/d = 75(●,●), and 100 (●,●), taken for the circular (a, c, e, C_μ^F = 3.1) and rectangular (b, d, f, C_μ^F = 3.2) jet, for yaw angles β = 0°– 90°.*

Quantification of the differences between the vortices induced by rectangular and circular jets is done in Figure 11 by estimates of the vortex circulation Γ in the x-z plane, the increment in the induced normal volume flow rate ΔQ through the vortex relative to the base flow, and the TKE levels within the vortex bounds, as an indication of the mixing induced by vortices. As it was done earlier, comparison between the jet configurations is done across the two most downstream planes (i.e., at x/d = 75 and 100) and for the varying yaw orientation. Comparing the CCW vortex circulation (Figures 11a and b), rectangular jet consistently induces between 30–50% higher circulation across 45° ≤ β ≤ 90°. It is noted that the rectangular jet circulation appears to level at the highest yaw angle, while that of the circular jet, albeit at lower level, does keep increasing through the full range of yaw angles. Both distributions follow the same trends between the x/d = 75 and 100, specific to the geometry. When comparing the volumetric flow rate gain, carried by the vortices (Figures 11c and d), a weaker dependence on the yaw angle is noted for the CCW vortex induced by the circular jet, although it does suggest there might be an optimum at about β = 45° (Figure 11c). Interestingly, there is a sharp drop in this gain with further increase in β, such that it reverts to a net loss (relative to the BL flow in the absence of the jet) at the highest yaw angle. While the corresponding distributions for rectangular jet similarly indicate an optimum level between β = 45° and 60°, suggesting not only a higher sensitivity to the jet yaw angle but also the peak levels 80% higher than for the circular jet, which is assisted by the larger CCW vortical structures in the case of rectangular jet (c.f., Figures 9 and 10). Similarly, turbulent kinetic energy levels $q = \left(\overline{u'^2} + \overline{v'^2} + \overline{w'^2}\right)/2$ associated with CCW vortices point to much higher levels within the vortices induced by rectangular jet, at about twice as high levels. Also, while the q levels of the circular-induced CCW vortex virtually do not depend on β (Figure 11e), those of the rectangular jet-induced vortex indicate levels between β = 60° and 75° (Figure 11f). Lastly, since the dominant CCW vortex is still accompanied by the weak CW vortex in the last two measurement planes for the circular jet case, the CW vortex is also characterized in Figures 11a, c, and e. As suggested in discussion of Figure 10, quantification of all these three parameters for the CW vortex indicate multifold smaller magnitudes at x/d = 75 when compared with its CCW counterpart, only

to closely approach zeros at x/d = 100, indicating that the jet interaction region extends to about x/d = 100.

V. Near Field Jet Interaction

While all the flow characterizations presented so far point to significant differences in turbulent BL interactions with pitched and yawed circular and rectangular jets, this section considers the origin of these interactions, immediately downstream from the jet orifices. Right at the point of the jet issuance into the BL flow, there is a difference in how the inner-orifice vorticity is sheared into the BL flow. In principle, circular jet shears a complex vortical structure that is locally about the orifice organized azimuthally, thus nominally introducing all vorticity components into the flow. On the other hand, rectangular jet issues vorticity that is predominantly organized into two vortex lines, whose ratio of spanwise and streamwise components depend on the yaw orientation. A rise of organized vortical structures upon introduction of such vorticity by the jets was shown to be rather complex even for a case of a round transverse jet, i.e., a jet issuing normal to the flow (e.g., Fric and Roshko, 1994, Kelso, Lim, and Perry, 1996). However, to the first approximation, and following the folding of the vortex sheet argument by Kelso, Lim, and Perry (1996) the near-orifice differences between the windward and leeward jet boundaries cause the vortex sheet to fold inward from the upstream/windward side into the leeward side. This process generates two vortical structures that, after turning and reorienting, form the counter-rotating vortex pair that dominates the downstream flow beyond the jet-boundary layer interaction region. Since the details of the interactions between the initially sheared vorticity and the surrounding BL flow depend on the jet orientation, further analysis is done for the fixed yaw angle of β = 90°. As already stated in Section II, these near field measurements are done close to the jet orifice, at the sPIV planes at x/d = 4.7, 7.1, 9.5 and 11.8. These four flow fields are shown

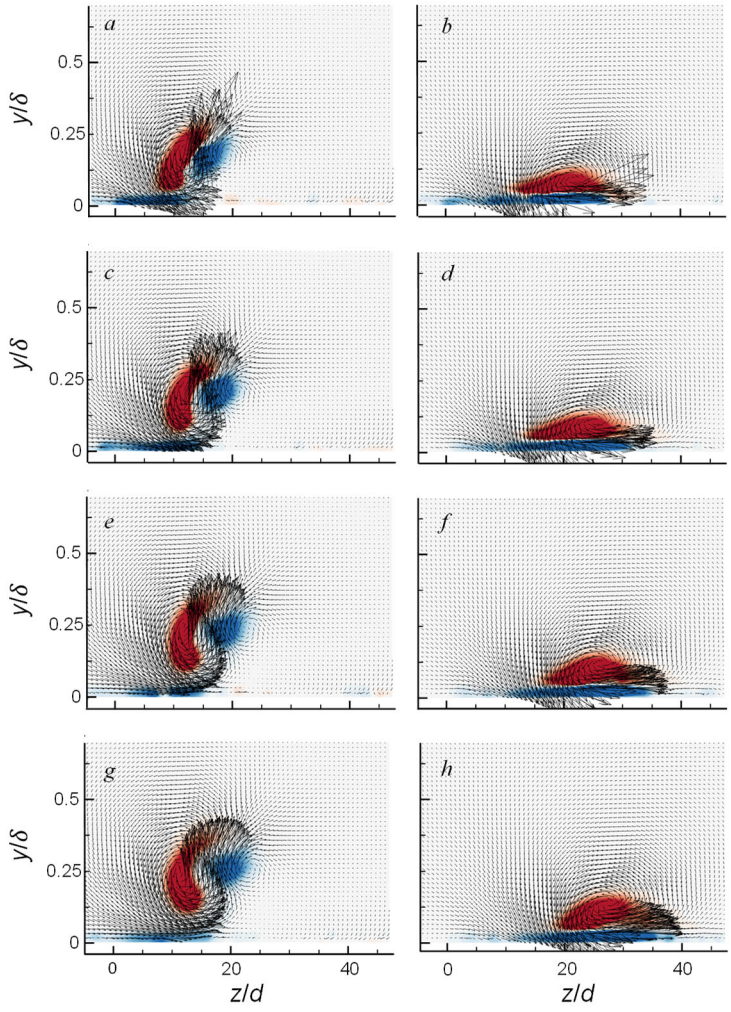

Figure 12. *Color raster plots of the mean streamwise velocity for the circular jet (C_μ^F = 3.1) at streamwise locations x/d = 4.7, 7.1, 9.5 and 11.8 (a, c, e, g) and rectangular jet (C_μ^F = 3.2) (b, d, f, h). Colorbar range is the same as in Fig. 4.*

in Figure 12 for the initial interaction of the circular and rectangular jets in terms of the mean streamwise vorticity component, having the mean in-plane velocity vectors overlaid over the color raster plots. When considering pitched/yawed circular jets, the top-level modification of the near-orifice folding of the vortex sheet is that there is a leading and the trailing section of the windward side of the jet, where the leading side would promote, and the trailing side would impede the folding process. While the interaction is considerably more complex, this simple modification of the folding argument implies asymmetry in the vortex pair formation, where the stronger one should originate from the leading side on the windward section of the jet. In the present experiments, where $45° \leq \beta \leq 90°$, the leading side in such orientations gives a rise to the CCW vortex. Indeed, the closest measurement plane ($x/d = 4.7$, Figure 12a) indicates stronger vorticity imprint on the CCW side, while the folding pair has a significant upward tilt, exceeding twice the initial jet pitch. Since the jet issues at $\beta = 90$, there is still a notable direct vortical CW contribution by the jet along the surface layer, in addition to the CCW and CW concentrations displaced off the surface. The successive downstream evolution of the vortex pair (Figures 12c, e, and g) indicates the transition from the folding vorticity sheets into the streamwise vortices, where their self-induced velocities also act to propel each other away from the surface. Since the CCW vortex is 'stronger' and of higher circulation, the CW vortex becomes displaced further with downstream evolution during this mutual interaction. The rectangular jet at the orientation $\beta = 90°$ has the orifice long sides aligned with the BL flow. Hence, its initial vortex sheet near the orifice has the vorticity predominantly aligned with the streamwise direction. It is argued that the low pitch angle in the case of rectangular jet creates a Coanda effect on the side of the vortex sheet carrying the CW sense of vorticity (pitch is in the $z+$ direction), which then promotes formation of a wall jet. As all of the vortical flow fields in Figures 12b, d, f, and h point to the same structure, having a folding vortex sheet only of the CCW sense (that originates on the z - side of the jet orifice), while the vorticity from the CW side remains confined to a layer along the surface, without being able to roll into a vortex. As the CCW sheet rollup into a vortex progresses in the downstream direction, along with the vortex-layer system shift sideways, the CW layer 'connection' to the jet origin ($z/d = 0$) weakens.

VI. Conclusions

The present experimental investigations focus on comparison of interactions of circular and rectangular surface jets having the same orifice areas with a nominally two-dimensional flat plate turbulent boundary layer ($Re_x = O(10^6)$], where the characteristic scales of the jet orifices are an order of magnitude smaller than the boundary layer thickness. Each surface jet issues at a pitch angle $\alpha = 20°$ relative to the oncoming flow at a range of yaw angles $45° \leq \beta \leq 90°$. Of specific interest are the cross stream and spanwise effects of the jets on distributions of cross stream momentum flux and momentum thickness near the surface relative to the baseline boundary layer (in the absence of jets), and the induced vortical structures within the flow. The actuation forces that are exerted by the jets are characterized by a bench test using the modified momentum coefficient C_μ^F that is based on the ratio of the jet thrust $\vec{F}$ magnitude measured in absence of cross flow, and the momentum flux across the boundary layer over the jet's characteristic scale. The evolution of the flow field near the surface in the absence and presence of the jets is measured using stereo PIV in streamwise-normal planes in the vicinity of the jet orifices within $4.7 < x/d < 11.8$ and farther downstream within $25 < x/d < 100$.

The present investigations demonstrated that the interactions of the jets with the cross-flow boundary layer differ significantly with orifice geometry. The circular jet penetrates and bends

within the cross flow up to $y/\delta \approx 0.6$ and leads to the formation of a counter-rotating vortex pair that is advected with the cross flow and whose symmetry varies with the yawing angle of the where the CCW vortex becomes dominant with increasing yaw angle. However, the evolution of the flow in the presence of the rectangular jet whose major axis forms the yaw angle relative to the cross flow is substantially different. As a result of an apparent Coanda effect along the orifice's long side at this shallow pitch angle, the jet forms as a wall jet along the surface. The jet is accompanied by the formation of a single sense CCW ($\beta > 0$) surface-bound streamwise vortex when the vorticity concentration that issues along the edge of the rectangular orifice is pulled atop of the CW vorticity layer on the opposite edge to form a dominant streamwise vortex that intensifies with increasing β. These differences in the evolutions of the jets within the cross flow and in the formation of the jet-induced streamwise vortices are manifested in their effects on streamwise momentum flux, entrainment, and mixing in the surrounding boundary layer. It is demonstrated that for a given actuation momentum coefficient C_μ^F, the effects of the rectangular jet on enhancement of momentum flux within the lower regions of the boundary layer is significantly more pronounced than the corresponding effects by the circular jet. Furthermore, despite its proximity to the surface, the streamwise decay rate of the surface-bound streamwise vortex that is formed by the rectangular jet is lower compared to that for the vortices formed by the circular jet. While redistribution of jet-effected momentum flux with increasing yaw orientation is intensified for both jets, the rectangular jet typically leads to 30-50% higher circulation, inducing higher gain in momentum flux, entrainment and mixing.

Acknowledgment/Disclaimer

This work was sponsored by the Office of Naval Research (ONR), under grant number N000142312500. The views and conclusions contained herein are those of the authors only and should not be interpreted as representing those of ONR, the U.S. Navy, or the U.S. Government. The authors also want to acknowledge assistance of Dr. Derek Nichols with some data post-processing tools and procedures.

References

Berson, A., Michard, M., and Blanc-Benon, P., "Vortex identification and tracking in unsteady flows," *Comptes Rendus Mécanique,* Vol. 337, No. 2, 2009, pp. 61-67.

Bray, T. P. and Garry, K. P. "Optimisation of Air-Jet Vortex Generators with Respect to System Design Parameters," *The Aeronautical Journal*, Vol. 103, No. 1028, 1999, pp. 475–479.

Compton, D. A., and Johnston. J. P., "Streamwise Vortex Production by Pitched and Skewed Jets in a Turbulent Boundary Layer," *AIAA Journal*, Vol. 30, No. 3, 1992, pp. 640-647.

Feng, Y-Y., Song, Y-P., and Breidenthal, R. E., "Model of the Trajectory of an Inclined Jet in Incompressible Crossflow," *AIAA Journal*, Vol. 56, No. 2, 2018, pp. 458-464.

Fric, T. F., and Roshko, A., "Vortical Structure in the Wake of a Transverse Jet," *Journal of Fluid Mechanics*, Vol. 279, 1994, pp. 1–47.

Godard, G., Foucaut, J. M., and Stanislas, M., "Control of a Decelerating Boundary Layer. Part 2: Optimization of Slotted Jets Vortex Generators," *Aerospace Science and Technology*, Vol. 10, No. 5, 2006, pp. 394–400

Graftieaux, L., Michard, M., and Grosjean, N., "Combining PIV, POD and vortex identification algorithms for the study of unsteady turbulent swirling flows," *Measurement Science and*

Technology, Vol. 12, No. 9, 2001, pp. 1422-1429.

Gutmark, E. J., and Grinstein, F. F., "Flow Control with Noncircular Jets," *Annual Review of Fluid Mechanics*, Vol. 31, 1999, pp. 239–272.

Johnston, J., Nishi, M., Vortex generator jets — means for flow separation control, *AIAA Journal,* Vol. 28, 1990, pp. 989–994.

Johnston, J.P. "Pitched and Skewed Vortex Generator Jets for Control of Turbulent Boundary Layer Separation: A Review," Proceedings of the 3rd ASME/JSME Joint Fluids Engineering Conference, FEDSM99-6917, 1999.

Karagozian, A.R., "The Jet in Crossflow," *Physics of Fluids*, Vol. 26, No. 10, 2014, pp.1-47.

Kelso, R. M., Lim, T. T., and Perry, A. E., "An Experimental Study of Round Jets in Crossflow," *Journal of Fluid Mechanics*, Vol. 306, 1996, pp. 111–144.

Mahesh, K., "The Interaction of Jets with Crossflow," *Annual Review of Fluid Mechanics*, Vol. 45, 2013, pp. 379-407.

Margason, R. J., "Fifty Years of Jet in Crossflow Research," In Computational and Experimental Assessment of Jets in Cross Flow, *AGARD-CP-534*, 1993.

Milanovic, I. and Zaman, K. B. M. Q. "Highly Inclined Jets in Cross Flow," *AIAA Paper 2003-183*, 2003.

Rixon, G. S. and Johari, H. "Development of a Steady Vortex Generator Jet in a Turbulent Boundary Layer," ASME. *J. Fluids Eng*., Vol. 125, No. 6, 2003, pp. 1006–1015.

Sharmishtha, C. and Utpal, B., "Review of Jets in a Cross Flow-Experimental and Numerical Approach," *International Journal of Engineering and Advanced Technology*, Vol. 7, No. 2, 2017, pp. 114-128.

Toth, B., Nichols, D.A., Vukasinovic, B., Glezer, A., DeFore, M.C., and Harris, C., "The Evolution of Streamwise Vortices Formed by Inclined and Swept Round Jet within a Turbulent Boundary Layer," AIAA Paper 2024-3634, 2024.

Tricouros, F., Amitay, M., and Van Buren, T., "A Parametric Study of Rectangular Jets Issuing into a Laminar Crossflow," *Experiments in Fluids*, Vol. 64, 2023

Zhang, X. "An Inclined Rectangular Jet in a Turbulent Boundary Layer—Vortex Flow," *Experiments in Fluids*, Vol. 28, 2000, pp. 344–354.